Four-wave-mixing spectroscopy of Cr-doped garnet crystals

Faqir M. Hashmi, Keith W. Ver Steeg, Frederic Durville, and Richard C. Powell
Center for Laser Research, Oklahoma State University, Stillwater, Oklahoma 74078-0444

G. Boulon
Universite Claude Bernard Lyon I, F-69622 Villeurbanne CEDEX, France
(Received 5 March 1990)

The characteristics of the four-wave-mixing signal of Cr^{3+} ions were measured for host crystals of $Gd_3Sc_2Ga_3O_{12}$, $Gd_3Ga_5O_{12}$, $(Gd,Ca)_5(Ga,Mg,Zr)_2Ga_5O_{12}$, and $La_3Lu_2Ga_3O_{12}$. Signal strengths and decay times were measured as functions of laser-beam crossing angles and temperature. The results are used to determine the properties of radiationless decay and energy-transfer processes in these samples. By comparing the characteristics of the $^4T_2$-^2E radiationless relaxation process among these and previously investigated Cr^{3+}-doped laser crystals, it is shown that the ratio of the intersystem-crossing relaxation rate to the internal conversion relaxation rate decreases as the strength of the crystal field of the host material decreases. The properties of energy migration among the Cr^{3+} ions in the different host materials is found to depend on the average separation of the Cr^{3+} ions, the strength of the crystal field, and the electron-phonon interactions.

I. INTRODUCTION

The use of garnet crystals such as $Gd_3Ga_5O_{12}$ (GGG) and $Gd_3Sc_2Ga_3O_{12}$ (GSGG) doped with Cr^{3+} and/or Nd^{3+} as laser materials has stimulated an interest in the study of the physical properties of these and similar garnets. A good deal of research has been directed towards the study of material characteristics essential to lasing.[1-9] These characteristics can be altered by changing the material's composition. This can be accomplished by studying other garnets such as $La_2Lu_3Ga_3O_{12}$ (LLGG) or by additional doping of optically inert ions. One attempt at the latter approach is substituting Ca^{2+}, Mg^{2+}, and Zr^{3+} ions for some of the Gd^{3+}, and Ga^{3+} ions in GGG to give a mixed garnet structure designated GGGM.[8,10] An understanding of how the crystal structure affects the dephasing and energy-transfer characteristics of the optically active ions is therefore essential. To this end, four-wave-mixing (FWM) spectroscopy is a useful tool. Previous studies of the spectroscopic properties as well as preliminary FWM results on GGG, GSGG, and GGGM have been reported.[9,11] This paper extends the previous work by using FWM to study energy migration and optical dephasing of Cr^{3+} ions by pumping into the $^4T_2$ band in GGGM, GGG, and GSGG, and by pumping into the $^4T_1$ band in LLGG. The results are compared to those obtained previously on Cr^{3+} ions in other laser crystals.

As reported in Ref. 10, the substitution of Zr^{3+}, Ca^{2+}, and Mg^{2+} ions for Ga^{3+} and Gd^{3+} ions in GGG results in a relatively high segregation coefficient of 2.8 and a larger lattice constant of 12.4942 Å. This produces a lower crystal field at the site of the dopant ion which is intermediate between the crystal-field values for GGG and GSGG. In addition, there are several nonequivalent sites for the Cr^{3+} ions which causes spectral structure and significant inhomogeneous broadening of the optical transitions. The sample used in this study, provided by the Chrismatec company in France, was $4\times4\times5$ mm^3 with a concentration of 5.4×10^{19} Cr^{3+} ions/cm^3. The GSGG and GGG samples were 5.5- and 1.5-mm thick with Cr^{3+} concentrations of 1.4×10^{20} and 1×10^{20} cm^{-3}, respectively. The LLGG sample was approximately $20\times10\times4$ mm^3, with the large flat surfaces perpendicular to the [111] direction, and a concentration of 5.0×10^{19} Cr^{3+} ions/cm^3.

Figures 1 and 2 show the room-temperature absorption and emission spectra of the GGGM and LLGG samples. The absorption spectra, taken by an IBM 9430 uv-visible spectrometer, are dominated by two strong absorption bands, centered at 460 and 640 nm in GGGM and 485 and 685 nm in LLGG. In both samples, the higher-energy band is due to the $^4A_2$-$^4T_1$ absorption transition

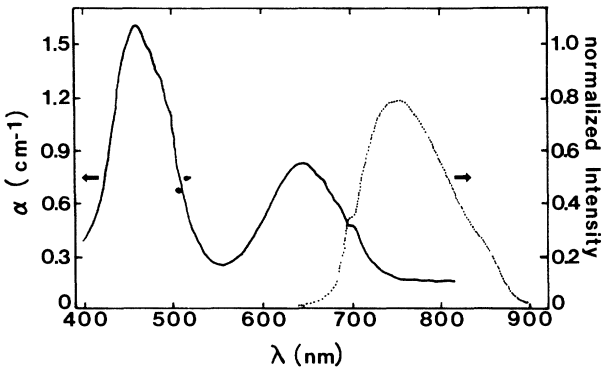

FIG. 1. Room-temperature absorption (solid line) and emission spectrum (dotted line) of Cr^{3+}-doped GGGM.

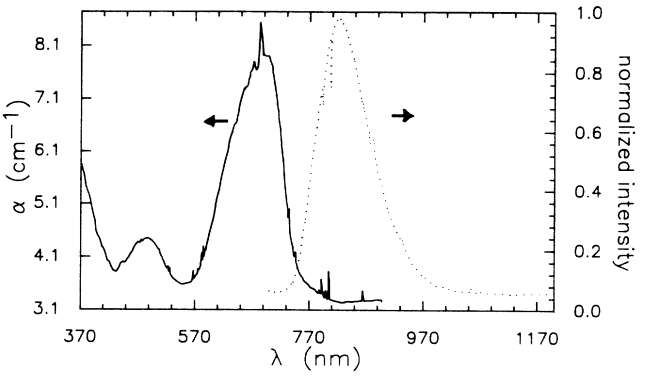

FIG. 2. Absorption (solid line) and emission spectrum (dotted line) of Cr^{3+}-doped LLGG at 12 K.

and the lower-energy band results from the $^4A_2$-$^4T_2$ transition. The sharp, relatively weak, spin forbidden transitions from the $^4A_2$ ground state to the ^{2}E, $^2T_1$, and $^2T_2$ states are overlapped by the broad bands. The transition matrix elements interfere destructively on one side of the sharp transition resonance and constructively on the other. This results in the absorption spectra having a characteristic antiresonant line shape, or Fano resonance, in the vicinity of the overlap. For GGGM, the dips in the lineshape on the low-energy side of the $^4T_1$ and $^4T_2$ bands are due to overlap with the sharp $^2T_2$ and $^2T_1$ transitions. The zero phonon line due to the $^4A_2$-^2E absorption is located at 695 nm. For LLGG, the lower crystal-field results in the $^4T_1$ and $^4T_2$ bands shifting towards lower energy. The antiresonances due to $^2T_1$ and $^2T_2$ therefore appear on the high-energy side of the two broad absorption bands. The prominent antiresonance near the peak of the $^4T_2$ band is due to the $^4A_2$-^2E transition. The other sharp lines in the spectrum correspond to the transitions of Nd^{3+}, which is an unwanted impurity.

The emission spectrum was excited by a nitrogen laser-pumped dye laser, analyzed with a 1-m spectrometer, and detected by an RCA C31034 photomultiplier tube for the GGGM and an RCA 7102 for the LLGG. The fluorescence for both samples is characterized by a very broad, Stokes shifted emission which is the result of the low crystal field causing the $^4T_2$ energy level to be lowered; in the case of LLGG, $^4T_2$ is 1000 cm^{-1} lower than ^2E as measured from minima to minima on the configuration coordinate diagram. For GGGM, the $^4T_2$-$^4A_2$ emission is centered at 750 nm with the ^2E-$^4A_2$ transition manifesting itself as a shoulder at 695 nm. For LLGG, the fluorescence is centered at 820 nm with the sharp dips and peaks due to Nd^{3+} impurities. For excitation at both 490 and 685 nm, the fluorescence decay of LLGG was single exponential, with the corresponding lifetime ranging from 120 μs at 11 K to 70 μs at room temperature. This is consistent with the fluorescence being dominated by emission from the $^4T_2$ level rather than the long-lived metastable ^2E level. Although the absorption at the peak of the $^4T_2$ band is about twice that at the peak of the $^4T_1$ band, the fluorescence intensity resulting from excitation at 685 nm is slightly less than the fluorescence from 490 nm excitation. This implies that some sort of fluoresence quenching occurs for excitation into the $^4T_2$ band. It is conceivable that a center other than the Cr^{3+} is being excited. However, analysis of the $^4T_2$ fluoresence shows an emission peak and lifetime consistent with excitation of Cr^{3+} which implies that the additional center must be nonfluorescing. We are unable to conclusively explain these results at the present time, although it appears that fluoresence quenching of the $^4T_2$ band may be the reason why no laser-induced grating is observed when exciting into this level, as discussed in the following.

II. RESULTS FOR FOUR-WAVE-MIXING SPECTROSCOPY

FWM is an effective method for studying long-range energy migration and optical dephasing phenomenon among dopant ions in solids.[12–14] Earlier papers[9,12,14] describe in detail the procedure for using FWM techniques as a spectroscopic tool. Figure 3 shows the experimental setup used in these experiments. Emission from a Spectra Physics argon ion laser or argon ion laser-pumped ring dye laser was passed through a chopper (CH) and divided into two beams of equal intensities using a 50:50 beam splitter (BS). These two noncollinear laser beams (called the write beams) are then focused onto the sample using the appropriate mirrors M_1, M_2, and M_3. The path length is adjusted so that the two write beams cross inside the sample creating a sinusoidal interference pattern. Since the energy of the laser photons is resonant with the energy of an electronic transition of the Cr^{3+} ions, an excited-state population grating is created having the same spatial pattern. This population grating produces a sinusoidal variation in the refractive index due to the difference in the polarizability of Cr^{3+} ions in the excited state versus the ground state. A very low power He-Ne laser beam nearly counterpro-

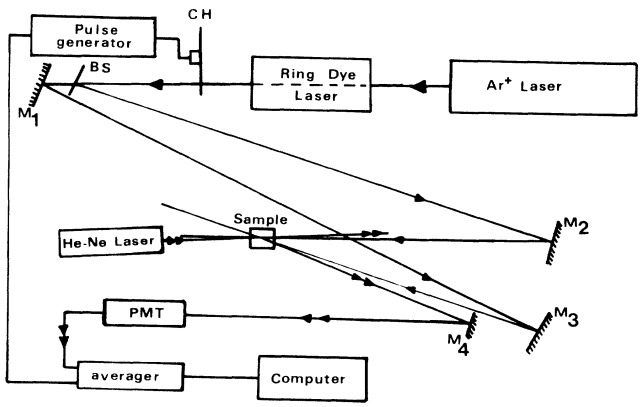

FIG. 3. Experimental setup for four wave mixing. CH—chopper BS—beam splitter and M—mirror. For excitation into the $^4T_1$ band, the ring dye laser is removed from the setup.

pagating to one of the write beams is scattered off this grating. When the Bragg condition is satisfied, the diffracted beam is nearly counterpropagating to the second write beam. This laser-induced grating (LIG) signal is then directed to an RCA C31034 photomultiplier tube (PMT) using mirror M_4. The output of the PMT is taken into an EG&G Princeton Applied Research model 4202 signal averager (averager) and then to an IBM XT personal computer where the digital data is stored. The trigger to the averager was provided by the chopper and pulse generator assembly. The sample was kept in a cryostat and the temperature was controlled using a CTI Cryogenics closed-cycle helium refrigerator and a Lake Shore Cryotronics model 805 temperature controller. The temperature measurements were accurate to better than 0.5 K.

The LIG signal carries all of the information about the physical processes influencing the population grating. Gratings were created by laser pumping into the $^4T_1$ band using an argon ion laser and pumping the $^4T_2$ band using an argon ion laser pumped dye laser. In both cases the population grating is observed after radiationless relaxation processes establish an equilibrium population in the ^2E and $^4T_2$ levels.

Figure 4 shows the intensity of the signal beam at room temperature for GGGM with 514.5 nm pumping. When both write beams are turned off at $t=0$, the signal decreases by a significant amount with a decay time of the order of the Cr^{3+} fluorescence lifetime indicating that the major contribution to the signal is associated with the Cr^{3+} population grating. The presence of a small residual signal indicates the presence of a long-lived grating, which is due to other physical processes such as charge relocation or the creation of color centers. To erase this long-lived grating, a single "erase beam" was turned on at $t=4$ min. Similar long-lived components to the LIG

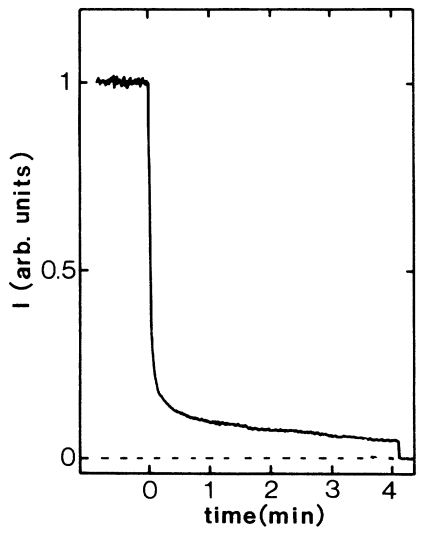

FIG. 4. LIG signal decay after the write beams are turned off at $t=0$ min, and after an erase beam is turned on at $t=4$ min.

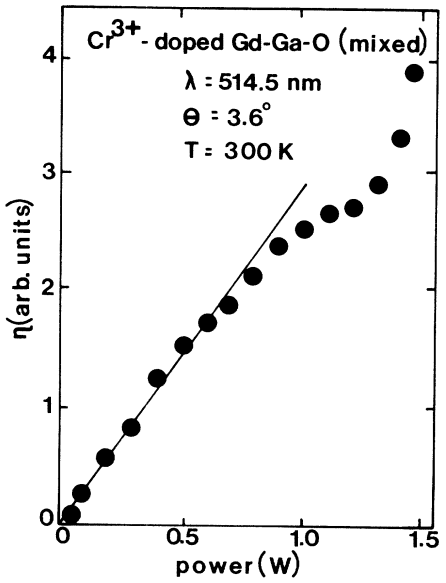

FIG. 5. Scattering efficiency as a function of laser beam power for excitation into the $^4T_1$ band of Cr^{3+}-doped GGGM.

signals were observed in the GGG and GSGG samples[9] but no long-lived grating component was observed for the LLGG sample. The characteristics of the signal beam associated with the population grating are discussed in the following.

The scattering efficiency for GGGM is plotted as a function of write beam power in Fig. 5. It was found to vary quadratically for low values of power, saturate for intermediate powers and then rise again for higher powers. The saturation occurs at power levels where the rate of pumping ions into the metastable state is equal to the fluoresence decay rate of the metastable state. The quadratic dependence and saturation level are consistent with the predicted behavior for this type of population grating.[14] The behavior at higher laser power indicates the onset of additional nonlinear optical processes. In order to ensure the validity of the results in the following sections, the write beam powers were kept low enough that the system was well below saturation.

A. Energy transfer

The decays of the LIG signal in GGGM were recorded at temperatures between 18 K and room temperature for both 514.5 and 581 nm excitation at various crossing angles of the write beams. The decay of the transient signal is shortened by energy migration from the peak to the valley region of the grating. As the crossing angle of the write beams is increased, the grating spacing is decreased and the effects of energy transfer are enhanced. The grating spacing Λ is given by

$$\Lambda=\lambda/[2\sin(\theta/2)]\ , \tag{1}$$

where θ is the write beam crossing angle. The crossing angles used here ranged from about 2° to about 22° giving

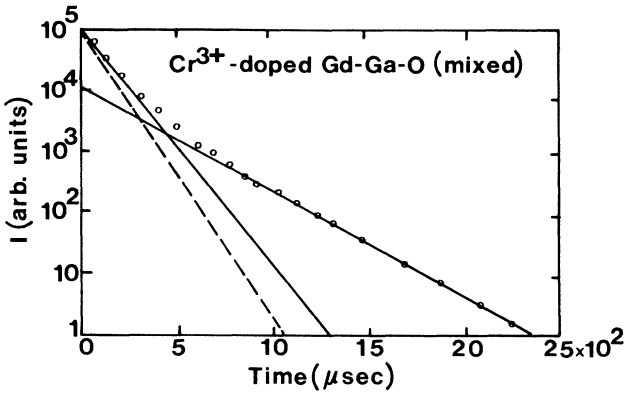

FIG. 6. Transient LIG signal decay at 18 K for Cr^{3+}-doped GGGM using 514.5 nm excitation. Total signal is shown to be comprised of two single exponentials.

a grating spacing ranging from about 1.4 μm to about 16 μm for the two wavelengths used.

Figure 6 shows an example of the decay of the transient LIG signal in GGGM. The decay is a double exponential which is consistent with the presence of two crystal-field sites for Cr^{3+} ions in the sample.[10] The decay times of the two components were found to have the same temperature and crossing angle dependences, therefore we show the analysis only for the short component.

Figure 7 shows an example of the signal decay rate in GGGM as a function of $\sin^2(\theta/2)$ for a given temperature. From the slope of the curve, we can calculate the exciton diffusion coefficient D for that temperature as described in the following. The temperature was varied from 18 to 300 K but no energy migration was observed for temperatures exceeding 150 K.

To obtain detailed information about the ion-ion interaction rate and exciton-phonon scattering rate, we have used the theory developed by Kenkre *et al.*[13] The basic assumptions used in the development of this model are consistent with the conditions of our experiments. According to this theory, exponential decays of the normalized transient grating signal in the presence of exciton migration can be described by

$$I_t(t)=\exp(-2t\{[(1/\tau_f+\alpha)^2+b^2]^{1/2}-\alpha\}) . \quad (2)$$

Here τ_f is the fluorescence lifetime, α is the exciton scattering rate, and b is defined as,

$$b=4V\sin[(2\pi a/\lambda)\sin(\theta/2)] , \quad (3)$$

where V is the nearest-neighbor ion-ion interaction rate, and a is the average distance between active ions. The exciton dynamics can be characterized by these parameters in terms of the diffusion coefficient D, the diffusion length L_d, the mean free path L_m, and the number of sites visited between successive scattering events N_s. These parameters are given by

$$D=2V^2a^2/\alpha , \quad (4)$$

$$L_d=(2D\tau_f)^{1/2} , \quad (5)$$

$$L_m=\sqrt{2}Va/\alpha , \quad (6)$$

$$N_s=L_m/a , \quad (7)$$

respectively. Table I shows the energy migration parameters for Cr^{3+} in GGGM determined in these experiments.

In Fig. 8, the exciton diffusion coefficient D is plotted as a function of temperature. The data can be fit by an expression of the form

$$D=A+(B/\sqrt{T}) , \quad (8)$$

which is consistent with phonon scattering limiting the mean free path of the exciton migration.[15]

Figure 9 shows the temperature dependences of the ion-ion interaction rate and the exciton-phonon scattering rate for GGGM. The ion-ion interaction rate is independent of the temperature while the exciton-phonon scattering rate increases linearly with temperature. This

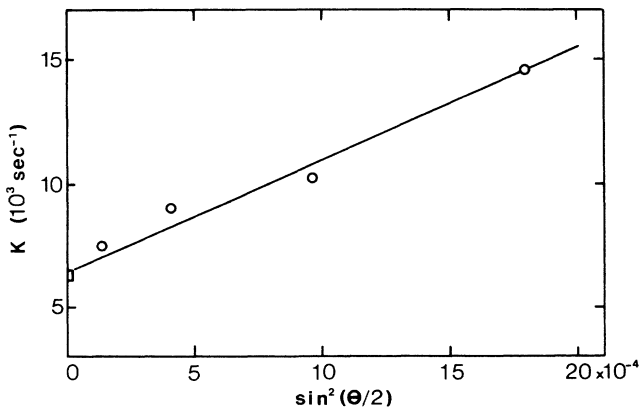

FIG. 7. FWM signal decay rate as a function of $\sin^2(\theta/2)$ for Cr^{3+}-doped GGGM. The point at $\theta=0$ is twice the measured fluorescence decay rate.

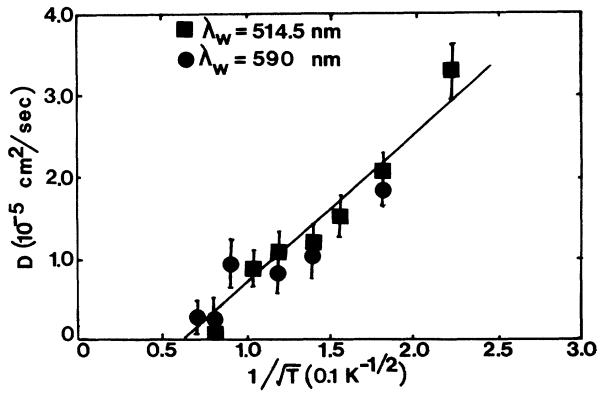

FIG. 8. Variation of the exciton diffusion coefficient D with respect to the temperature for Cr^{3+}-doped GGGM.

TABLE I. Energy migration parameters for Cr^{3+}-doped GGGM.

T(K)	$\alpha(10^4\ \text{sec}^{-1})$	$V(10^6\ \text{sec}^{-1})$	$D(10^{-5}\ \text{cm}^2/\text{sec})$	$L_m(\mu\text{m})$	$L_d(\mu\text{m})$
18	1.160	4.186	6.41	0.74	15.81
30	1.303	4.206	5.76	0.65	15.18
40	1.968	3.760	3.05	0.39	11.05
50	3.493	4.190	2.14	0.25	9.25
70	5.024	3.830	1.24	0.15	6.86
90	7.159	4.085	0.99	0.12	6.29
110	10.350	3.980	0.65	0.08	4.84
150	11.210	4.060	0.31	0.07	3.34

increase is associated with the additional phonons available at higher temperatures.

Similar studies on LLGG revealed that when exciting the $^4T_1$ band at 488 nm, the transient grating decay rate was independent of the angle between the write beams at all sample temperatures between 25 and 220 K. This is consistent with no long-range energy migration occurring in this material. No FWM signal could be observed when exciting the $^4T_2$ band at 660 nm.

B. Optical dephasing measurements

The laser beams in a FWM experiment drive the system of ions coherently and the time it takes the system of ions to lose phase coherence affects the strength of the FWM signal. Dephasing can occur when the ions interact with the phonons of the system or with other ions in the ensemble or when decay to another energy level occurs. The model used to describe the effect of dephasing on the FWM signal was developed in Refs. 16, 17, and 18 and extended for our experimental conditions in Refs. 12 and 14. The main assumption of this model is the approximation of the ensemble of ions as a two-level system.

The model describes an ensemble of two-level systems and their interaction with the four laser beams through four coupled differential equations. These equations have been solved numerically treating the real and imaginary parts of the coupling parameters D_1 and D_2 as adjustable parameters defined below:

$$D_1 = D_1^r + iD_1^i = 2\pi\mu L(\kappa - \xi) , \tag{9}$$

$$D_2 = D_2^r + iD_2^i = \pi\mu\Delta\kappa L , \tag{10}$$

where μ is the permeability of the material, ξ is an effective susceptibility, L is the distance of the overlap region, κ is a parameter related to the complex index of refraction, and $\Delta\kappa$ is the laser induced modulation of κ. This can be separated into a modulation Δn of the refractive index and $\Delta\alpha$ of the absorption coefficient. These parameters are related to the adjustable coupling parameters D_1^r, D_1^i, D_2^r, and D_2^i as follows:

$$\Delta\alpha = -2\bar{\alpha}D_2^i/D_1^i , \tag{11}$$

$$\Delta n = (\bar{\alpha}c/\omega)D_2^r/D_1^i , \tag{12}$$

where ω is the frequency of the laser line, $\bar{\alpha}$ is the average absorption coefficient at the write beam wavelength and c is the speed of light. The dephasing time, T_2 is given by

$$T_2 = (2\omega/c)(\Delta n/\Delta\alpha)(\omega - \omega_{21})^{-1} , \tag{13}$$

where ω_{21} is the resonant transition frequency.

The set of coupled differential equations can be solved for special cases.[12] To see the effect of the crossing angle on the scattering efficiency, we consider one special case where,

$$(D_2^i)^2 + (D_2^r)^2 - (D_1^i + D_2^i)^2 > 0 \tag{14}$$

and

$$D_1^r - D_2^r \neq \begin{cases} 0 \\ [(D_2^r)^2 + (D_2^r)^2 - (D_1^i - D_2^i)^2]^{1/2} \end{cases} . \tag{15}$$

The scattering efficiency is then given by

$$\eta(\theta) = 2[(D_2^i)^2 + (D_2^r)^2][(D_2^i)^2 + (D_2^r)^2 - (D_1^i + D_2^i)^2]^{-1} \times \sin^2\{k[(D_2^r)^2 + (D_2^r)^2 - (D_1^i + D_2^i)^2]^{1/2} \times \ln[\tan(\theta/4)]\} . \tag{16}$$

The crossing angle θ in the preceding expression is directly connected with the overlap of the laser beams which in turn determines the modulation of the complex index of

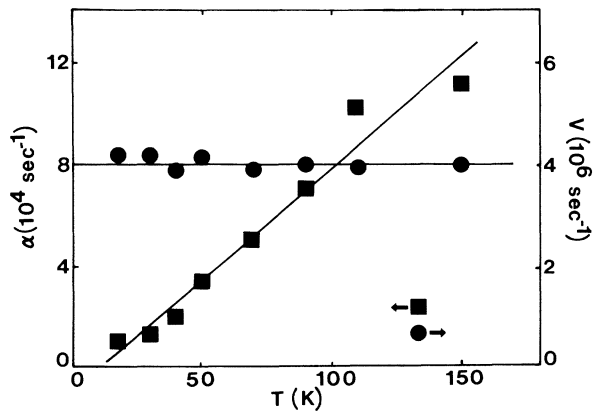

FIG. 9. Variation of the exciton-phonon scattering rate α and ion-ion interaction rate V as functions of temperature for Cr^{3+}-doped GGGM.

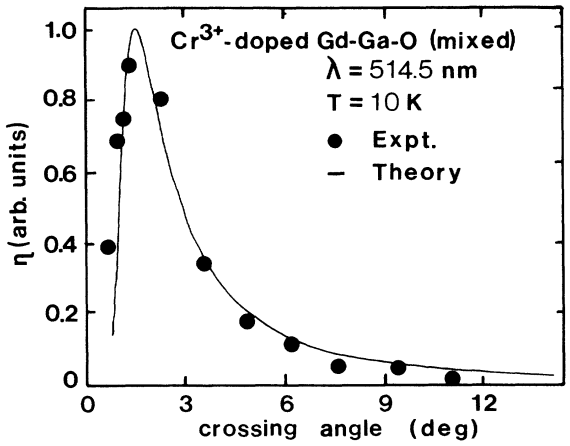

FIG. 10. LIG scattering efficiency as a function of crossing angle of the write beams for excitation into the $^4T_1$ band of Cr^{3+}-doped GGGM.

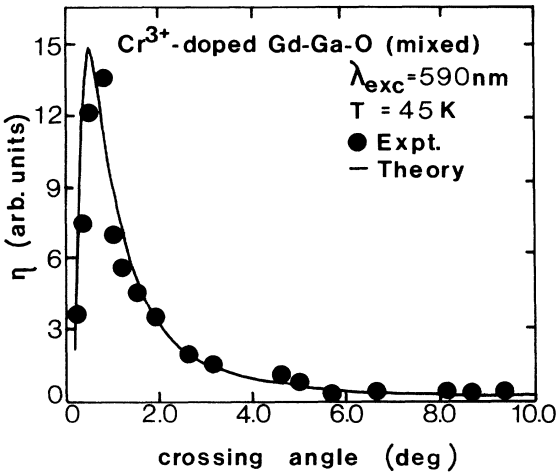

FIG. 11. LIG scattering efficiency as a function of crossing angle of the write beams for excitation into the $^4T_2$ band of Cr^{3+}-doped GGGM.

refraction and the absorption coefficient. The coefficients in the expression for η are found numerically.

In Fig. 10 the scattering efficiency is plotted as a function of the crossing angle for excitation into the $^4T_1$ band of GGGM. Solid circles represent the experimental data points whereas the solid line denotes the theoretical fit. The good agreement between theory and experiment shows that for write beam powers well below saturation,

TABLE II. Parameters for the best fit to the scattering efficiency vs crossing angle plot and the dephasing time T_2 for Cr^{3+}-doped laser materials. NA indicates that the data is not available.

Material and transition	D_1^r	D_1^i	D_2^r	D_2^i	T_2 (ps)
Alexandrite (Ref. 12) (inversion) $^4T_2$	0.006	0.015	0.135	0.000 02	80±5
Ruby (Ref.12) $^4T_2$	NA	NA	NA	NA	4.5±3
Alexandrite (Ref. 12) (mirror) $^4T_2$	NA	NA	NA	NA	2.2±4
Alexandrite (Ref. 14) (mirror) ^2E	0.250	0.650	0.350	0.0015	55.3
Emerald (Ref. 29) $^4T_2$	5.0×10^{-7}	4.0×10^{-7}	2.0×10^{-6}	8.0×10^{-9}	1.2
GGG $^4T_2$	0.205	0.20	0.230	0.0007	1.35±0.5
GGG (Ref. 9) $^4T_1$	0.2−0.45	0.09−0.2	0.27−0.31	0.01−0.05	0.008−0.033
GSGG $^4T_2$	0.210	0.18	0.240	0.001	0.77±0.5
GSGG (Ref. 9) $^4T_1$	0.30	0.30	0.31	0.01	0.033
GGGM $^4T_1$	0.92	0.01	0.100	0.05	0.0028±0.0005
GGGM $^4T_2$	0.200	0.22	0.235	0.001	0.92±0.5
LLGG $^4T_1$	0.400	0.280	0.303	0.015	0.74±0.5

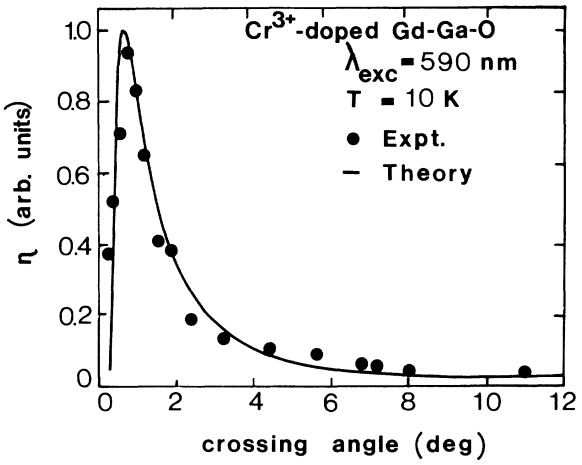

FIG. 12. Scattering efficiency as a function of crossing angle for the excitation into $^4T_2$ band of Cr^{3+} ions in Cr^{3+}-doped GGG.

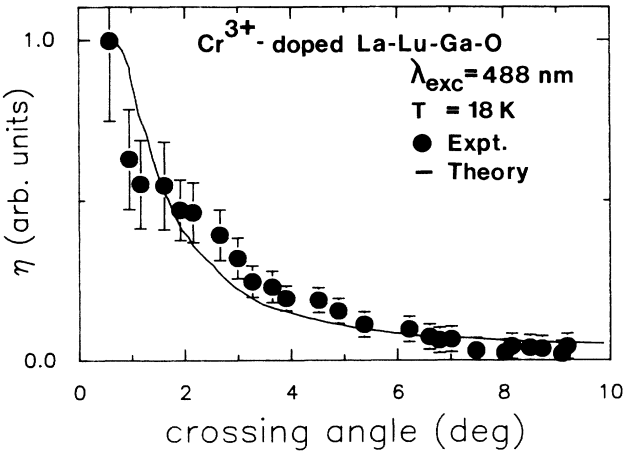

FIG. 14. LIG scattering efficiency as a function of crossing angle of the write beams for excitation into the $^4T_1$ band of Cr^{3+}-doped LLGG.

the two-level system gives a reasonable description of the results. The values of the parameters used to obtain the best fit along with the calculated dephasing times for different materials used in this survey are given in Table II.

Figures 11–14 give the experimental data and theoretical fits for the scattering efficiencies as a function of the write beam crossing angle for the excitation into the $^4T_2$ band of GGGM, GGG, GSGG, and the $^4T_1$ band of LLGG, respectively. The values of the parameters used to obtain the best fit and the corresponding dephasing time are given in Table II.

The expression for the dephasing time T_2 is given by[18]

$$1/T_2 = 1/T_1 + 1/T_2^{PD} , \tag{17}$$

where T_1 is the relaxation time of the excited level and T_2^{PD} is the time associated with the scattering mechanisms.

For excitation into the $^4T_2$ band, the dephasing is dominated by the time an ion takes to relax to the metastable ^2E level. This relaxation can follow two possible paths as described by the model proposed by Gilliland *et al.*[14] Figure 15 (adopted from Ref. 14) shows the energy-level parabolas for Cr^{3+} ions. The laser excites an ion into an excited vibrational level of the $^4T_2$ band at point *A*. It

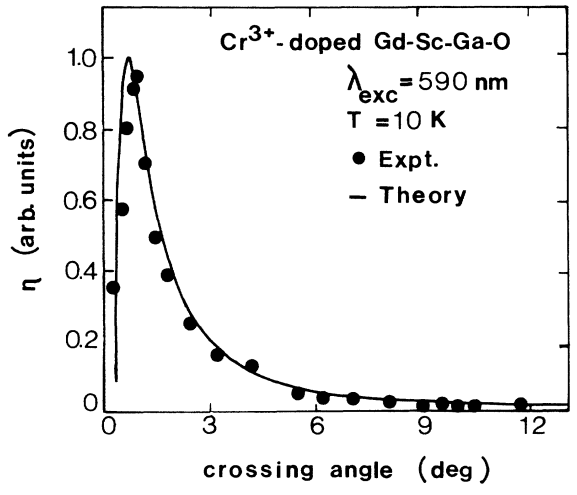

FIG. 13. LIG scattering efficiency as a function of crossing angle of the write beams for excitation into the $^4T_2$ band of Cr^{3+}-doped GSGG.

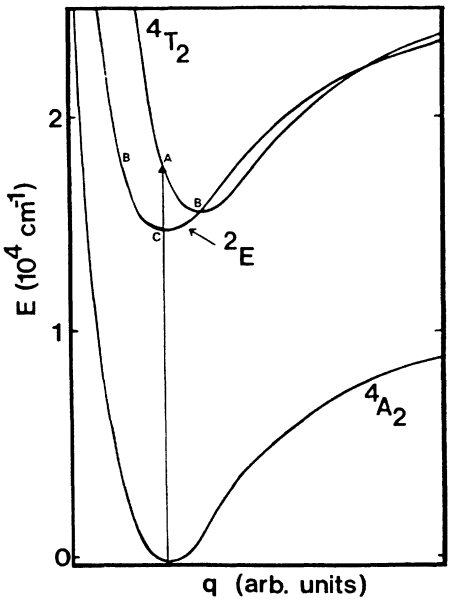

FIG. 15. Model used to analyze the dynamics of the nonradiative decay from the $^4T_2$ level to the ^2E level of Cr^{3+} ions in Alexandrite. The solid vertical line represents optical absorption (adopted from Ref. 14).

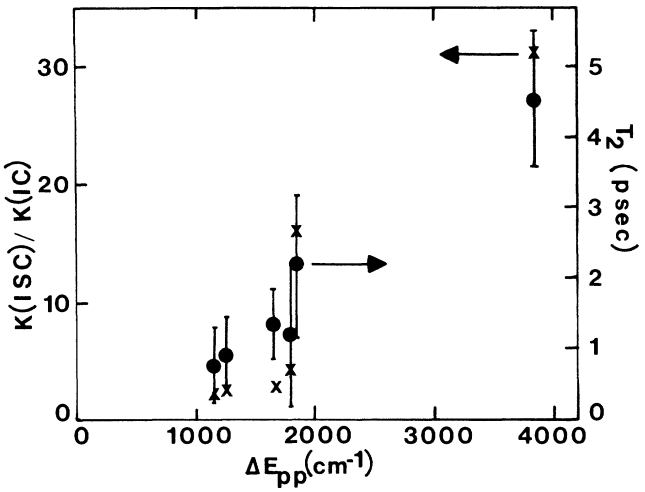

FIG. 16. T_2-dephasing time and the ratio K_{nr} (ISC)/K_{nr}(IC) as a function of ΔE_{pp} (the energy difference between the peak of the $^4T_2$ band and the peak of the ^2E band in the absorption spectrum of Cr^{3+}-doped laser materials).

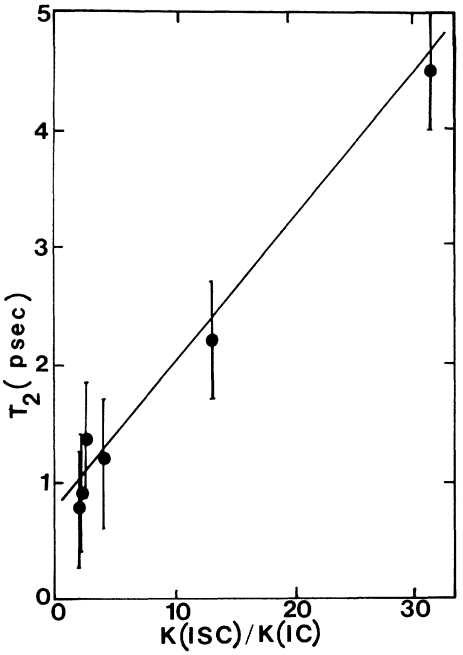

FIG. 17. Dephasing time (T_2) as a function of the ratio K(ISC)/K(IC).

can then relax within the $^4T_2$ band following the path through point B (where the two parabolas cross). The excitation then crosses over to the ^2E state and emits phonons until it reaches the bottom of the ^2E potential well. This process is called internal conversion (IC) and the corresponding nonradiative rate is denoted by K_{nr} (IC). Alternatively, the excited ion can relax by immediately crossing over to the ^2E band at point B' and then emitting phonons to reach the bottom of the potential well. This process is called intersystem crossing (ISC) and the corresponding nonradiative rate is denoted by K_{nr} (ISC). As noted in Ref. 14, after the first step is taken, the entire path for the dephasing is determined. The dephasing time T_2 is directly affected by whether IC or ISC path is the preferred channel for the nonradiative relaxation. Since the details of this process are described in Ref. 14, we will only mention the important points.

The nonradiative decay rates are calculated using standard perturbation theory techniques.[19] The vibrational matrix elements are calculated using a single effective phonon frequency and Morse potential wave functions to account for anharmonicity.[20–27] The multielectron reduced matrix elements involved here are expressed in terms of the single-electron reduced matrix elements which have already been tabulated by Sugano *et al.*[28] Due to the difficulties involved in calculating the exact electronic wave functions needed for the evaluation of the single-electron matrix elements, only the ratio of the two rates K_{nr}(ISC)/K_{nr}(IC) is considered.

Calculations were performed for the Cr-doped laser materials ruby, alexandrite, emerald, GGG, GGGM, and GSGG, which have been investigated by FWM spectroscopy. The results can be used to determine the relationship between the dephasing process and the energy

TABLE III. Results of dephasing time measurements on Cr^{3+}-doped laser materials for pumping into the $^4T_2$ band.

Material	ΔE_{pp} (cm^{-1})	K_{nr}(ISC)/K_{nr}(IC)	$\Delta\alpha$ (cm^{-1})	Δn (10^{-5})
Alexandrite (Ref. 12) (Inversion)	5500		0.001 1	2.52
Ruby (Ref. 12)	3850	31	0.001 06	8.16
Alexandrite (Ref. 12) (Mirror)	1950	13	0.001 9	1.83
Emerald (Ref. 29)	1800	4.0	0.22	13
GGG	1650	2.6	0.009 3	1.44
GGGM	1250	2.3	0.003 5	0.38
GSGG	1150	2.2	0.003 1	0.35

difference between the peak of the $^4T_2$ band and the peak of the ^2E band in the absorption spectrum denoted by ΔE_{pp}. Nonradiative decay rates were calculated for the two possible dephasing paths and results of the calculations are given in Table III.

It is interesting to note that for all the materials considered, the ratio $K_{nr}(ISC)/K_{nr}(IC)$ is greater than 1. This generalizes the conclusion drawn in Ref. 14 that in Cr-doped laser materials, after pumping into the $^4T_2$ level, the dominant relaxation path for the excitation is ISC and not IC.

In Fig. 16 the ratio $K_{nr}(ISC)/K_{nr}(IC)$ and the dephasing time are plotted as a function of the energy splitting ΔE_{pp}. The two quantities have the same dependence on ΔE_{pp}. To further demonstrate this relationship, the dephasing time T_2 is plotted as a function of the ratio $K_{nr}(ISC)/K_{nr}(IC)$ in Fig. 17 and the result is a straight line.

III. DISCUSSION AND CONCLUSIONS

Investigations of long-range energy migration have been carried out on several different Cr^{3+}-doped laser crystals. No long-range energy migration was observed in ruby, the inversion site ions in alexandrite, or LLGG. Detailed information on ion-ion interaction rates and exciton-phonon scattering rates was not available from the previous results reported for GGG and GSGG. Table IV summarizes the results for GGG, GSGG, GGGM, LLGG, emerald, ruby, and inversion and mirror site ions in alexandrite. The characteristics of energy transfer vary significantly from host to host depending on parameters such as the distance between the Cr^{3+} ions, the lifetime of the metastable state, the spectral overlap between absorption and emission, and the electron-phonon interactions. The variation of each of these parameters from host to host makes it difficult to establish a simple trend for energy transfer in Cr^{3+}-doped crystals.

One critical parameter in a diffusion or random walk picture of energy migration is the spacing between the sites of the lattice on which the random walk is occurring, designated as a. In this case a is the average separation between Cr^{3+} ions. This appears explicitly in the expression for both the ion-ion interaction rate V and the diffusion coefficient D. This separation is affected by the Cr^{3+} concentration in the sample, the host lattice spacings, and the distribution properties of the Cr^{3+} ions in the host. For mirror sites in alexandrite crystals, it is well known that the Cr^{3+} ions are not distributed randomly and the value of a used in Table IV was estimated from previous measurements on this sample.[12,14] For the

TABLE IV. Energy migration parameters for Cr^{3+}-doped laser crystals. NA indicates that the data is not available.

Material and transition	Dq (cm^{-1})	ΔE (cm^{-1})	D (10^{-8} cm^2/sec)	V (10^5 sec^{-1})	α (10^3 sec^{-1})	T (K)	a (A)	N (10^{18} cm^{-3})	L_d (10^{-6} m)
Alexandrite (inversion) $^4T_2$ (Refs. 12,14,31)	2200	6400	0	NA	NA	ALL	41	2.5	NA
Ruby ^2E (Ref. 35)	1820	2300	0	NA	NA	ALL	59−108	79−490	3
Alexandrite (mirror) ^2E (Refs. 14,31)	1680	800	3	12	200	25	27	8.9	12
Emerald $^4T_2$ (Refs. 29,34,35)	1620	400	28	1.9	2.6	12	10	177	31
GGG $^4T_1$ (Refs. 4,9)	1597	298	1	NA	NA	18	NA	140	NA
GGGM (Ref. 10)	1567	100	6410	42	12	18	15	54	16
GSGG $^4T_1$ (Refs. 4,9)	1565	50	10	NA	NA	230	NA	NA	NA
LLGG $^4T_1$	1480	−1000	0	NA	NA	ALL	15	50	NA

other samples, the values listed for a are the average Cr^{3+} separations assuming a uniform distribution of ions. This of course is a rough approximation to the true situation of randomly distributed impurity ions. Note that for the two high crystal-field cases of ruby and alexandrite inversion sites, the values of a are extremely large. This results in a very small value for V and thus explains the lack of long-range energy migration in these cases.

The samples in Table IV are listed in order of decreasing crystal field. As the crystal field decreases, the population distribution of the excited state of the Cr^{3+} ions changes from being primarily in the ^2E level to being primarily in the $^4T_2$ level. The latter level has a shorter lifetime and larger Stokes shift compared to the former level. The lifetime decrease results in an increase in V while the increased Stokes shift decreases the spectral overlap integral thus decreasing the number density of ions, N and V. The value of the ion-ion interaction rate decreases by an order of magnitude between alexandrite (M) and emerald and then increases by an order of magnitude between emerald and GGG. The fluorescence lifetime is not significantly different for alexandrite (M) and emerald samples so the observed decrease in V is associated with the decreased spectral overlap. The increase in the case of GGGM may, however, be associated with the smaller fluorescence lifetime in this sample. The increased values of D for these three samples is associated with the decreased values of α as well as changes in the number density of ions, N. The value of V was found to be essentially independent of temperature at low temperatures for alexandrite mirror sites and the GGGM sample indicating that α and N do not vary with T in this range. However, in emerald V was found to increase with temperature because N increases.[29] The temperature dependence of V was not determined for the other samples.

The values of the scattering rate α which limits the mean free path of the migrating energy varies from alexandrite (M) to GGGM and is found to increase with temperature. Since the details of the exciton-phonon coupling are not known, it is not possible to predict the sample-to-sample variation in α.

From the discussion above, it is possible to understand the observed differences in the energy diffusion coefficient D from sample to sample. The values of D increase with increasing ion-ion interaction rate and decrease with increasing excitation scattering rate. The diffusion coefficient increases with temperature in emerald where V is phonon assisted but decreases with temperature for alexandrite mirror sites and GGGM where V is constant and α increases with temperature. Recently Kaplyanskii has combined the techniques of site-electron spectroscopy and Stark shifting of spectral lines to distinguish between resonant and nonresonant energy transfer between Cr^{3+} ions at low temperature.[30] He observed "anomalously fast and effective" resonant energy transfer among the Cr^{3+} ions in mirror sites in alexandrite crystals but not in ruby crystals. His results are consistent with the results of FWM studies of energy migration in these samples.

Comparing the results obtained on the dependence of the FWM signal magnitude of the crossing angle of the write beams with the model proposed by Gilliland *et al.*[14] for the dephasing mechanism in Cr-doped materials, we conclude that internal conversion is the dominant relaxation path when the chromium ions are excited to the $^4T_1$ level. This is due to the fast relaxation of the excitation to the bottom of the $^4T_1$ configuration potential well. The information on optical dephasing obtained from FWM measurements pumping into the $^4T_2$ level shows that radiationless relaxation to the ^2E level through intersystem crossing is the dominant dephasing process in these Cr^{3+}-doped laser crystals. The relative importance of dephasing through internal conversion within the $^4T_2$ level becomes more important as the crystal field of the host decreases.

The analysis for determining the dephasing time, change in refractive index (Δn), and the change in absorption coefficient ($\Delta\alpha$) assumes an effective two-level system model. The use of this model, despite its simplicity, has been justified on the basis of its ability to predict values of $\Delta\alpha$ which are consistent with values determined independently by ground and excited-state absorption measurements. Such checks have been done when values of the excited-state absorption cross section σ_f are available, such as for alexandrite,[31] ruby,[32] GSGG,[33] and emerald.[34,35]

Recently, the results of FWM measurements on Nd^{3+}-doped materials has been analyzed using a model based on an effective four-level system.[36] In this model, the laser beams interact with ions both in the ground state and metastable state. The transitions from the ground and metastable states to higher-energy states is accounted for by combining the upper states into two effective states. A density matrix formalism yields the change in the real and imaginary parts of the nonlinear susceptibility between ions in the peak and valley of a population grating. By measuring the absolute magnitude of the FWM signal in a variety of samples, it was concluded that the dominant contribution to the signal comes from the real part of the nonlinear susceptibility associated with the off resonant, allowed transitions to the levels of different configuration in the ultraviolet spectral region. The relative values of Δn and $\Delta\alpha$ obtained in this work are consistent with the proposed model. In this case the weak contribution to the signal associated with the imaginary part of the nonlinear susceptibility comes from the resonant interaction with the pump transition. Recognizing the contributions due to these two different types of transitions, the expressions for Δn and $\Delta\alpha$ will be the same for the two-level and four-level modes.

It is important to note that the procedure for using the two-level system fit to the crossing angle dependence of the FWM scattering efficiency to find the dephasing time should be approached with caution. This approach has been justified on the basis that values found for $\Delta\alpha$ are in good agreement with those values found independently from excited-state absorption measurements. Equation (11) shows how $\Delta\alpha$ depends on the fitting parameter D_2^i; however, the computer fit to the crossing angle dependence of the FWM scattering efficiency can be relatively insensitive to the parameter D_2^i. This may result in large

error bars for $\Delta\alpha$ and thus a large error in the value determined for T_2 which is dependent on $\Delta\alpha$, as shown in Eq. (13).

Accurate confirmation of the values of T_2 determined by these FWM measurements must come from a direct measurement of the dephasing time. Photon echo measurements are currently being made on these Cr^{3+}-doped materials to determine T_2.

ACKNOWLEDGMENTS

This work was supported by a contract from the U.S. Army Research Office and by the National Science Foundation under Grant No. DMR-87-22350. The Université Claude Bernard Lyon I is Unité Associé No. 442 du Centre National de la Recherche Scientifique.

[1]B. Struve, G. Huber, V. V. Laptev, I. A. Scherbakov, and Y. V. Zharikov, Appl. Phys. B **28**, 235 (1982).
[2]B. Struve and G. Huber, J. Appl. Phys. **57**, 45 (1985).
[3]E. V. Zharikov, N. N. Il'ichev, V. V. Laptev, A. A. Malyutin, V. G. Ostroumov, P. P. Pashinin, and I. A. Shcherbakov, Sov. J. Quantum. Electron. **QE-12**, 338 (1982).
[4]B. Struve, G. Huber, Appl. Phys. B **36**, 195 (1985).
[5]E. V. Zharikov, V. V. Laptev, E. I. Sidorova, Yu. P. Timofeev, and I. A. Shcherbakov, Sov. J. Quantum Electron. **QE-12**, 1124 (1982).
[6]G. Huber and K. Petermann, in *Tunable Solid State Lasers*, edited by P. Hammerling, A. B. Budgore, and A. Pinto (Springer, Berlin, 1985), Vol. 47, p. 11.
[7]E. V. Zharikov, V. V. Osiko, A. M. Prokhorov, and I. A. Shcherbakov, Izv. Adad. Nauk SSSR Ser. Fiz. **48**, 1330 (1984).
[8]G. Boulon, C. Garapon, and A. Monteil, in *Advances in Laser Sciences II*, edited by M. Lapp, W. C. Stwalley, and G. A. Kenney-Wallace (AIP, New York, 1987), p. 87.
[9]Andrzej Suchocki and Richard C. Powell, Chem. Phys. **128**, 59 (1988).
[10]A. Monteil, C. Garapon, and G. Boulon, J. Lumin. **39**, 167 (1988).
[11]F. Durville, R. C. Powell, and G. Boulon, J. Phys. (Paris) Colloq. **48**, C7-517 (1987).
[12]A. Suchocki, G. D. Gilliland, and R. C. Powell, Phys. Rev. B **35**, 5830 (1987).
[13]V. M. Kenkre and D. Schmid, Phys. Rev. B **31**, 2430 (1985).
[14]Guy D. Gilliland, Andrzej Suchocki, Keith W. Ver Steeg, Richard C. Powell, and Donald F. Heller, Phys. Rev. B **38**, 6227 (1988).
[15]V. M. Agranovich and M. D. Galanin, *Electronic Excitation Energy Transfer in Condensed Matter* (North-Holland, Amsterdam, 1982).
[16]R. L. Abrams and R. C. Lind, Opt. Lett. **2**, 94 (1978).
[17]A. Yariv and D. M. Pepper, Opt. Lett. **1**, 16 (1977).
[18]M. D. Levenson, *Introduction to Nonlinear Laser Spectroscopy* (Academic, New York, 1982).
[19]Eugen Merzbacher, *Quantum Mechanics* (Wiley, New York, 1970).
[20]P. M. Morse, Phys. Rev. **34**, 57 (1929).
[21]B. I. Makshantsev, Opt. Spektrosk. **31**, 355 (1971) [Opt. Spectrosc. (USSR) **31**, 191 (1971)].
[22]M. D. Sturge, Phys. Rev. B **8**, 6 (1973).
[23]J. A. C. Gallas, Phys. Rev. A **21**, 1829 (1983).
[24]P. A. Fraser and W. R. Jarmain, Proc. Phys. Soc. London Sec. A **66**, 1145 (1953).
[25]J. A. C. Gallas, H. P. Grieneisen, and B. P. Chakarborty, J. Chem. Phys. **69**, 612 (1978).
[26]V. S. Vasan and R. J. Cross, J. Chem. Phys. **78**, 3869 (1983).
[27]R. Englman and B. Barnett, J. Lumin. **3**, 37 (1970).
[28]S. Sugano, Y. Tanabe, and H. Kamimura, *Multiplets of Transition Metal Ions in Crystals* (Academic, New York, 1970).
[29]Gregory J. Quarles, Andrzejl Suchocki, and Richard C. Powell, Phys. Rev. B **38**, 9996 (1988).
[30]S. A. Basun, A. A. Kaplyanskii, V. N. Matrosov, S. P. Feofilov, A. A. Chernyshev, and A. P. Shkadarevich, Opt. Spektrosk. **66**, 1067 (1989) [Opt. Spectrosc. (USSR) **66**, 624 (1989)].
[31]M. L. Shand, J. C. Wailing, and R. C. Morris, J. Appl. Phys. **52**, 953 (1981).
[32]W. M. Fairbank, Jr., G. K. Klauminzer, and A. L. Schawlow, Phys. Rev. B **11**, 60 (1975).
[33]L. J. Andrews, S. M. Hitelman, M. Kokta, and D. Gabbe, J. Chem. Phys. **84**, 5229 (1986).
[34]R. C. Powell, A. Suchocki, G. D. Gilliland, and G. J. Quarles, J. Lumin. **38**, 250 (1987).
[35]T. F. Veremeichik, Phys. Status Solidi B **124**, 719 (1984).
[36]R. C. Powell, S. A. Payne, L. L. Chase, and G. D. Wilke, Phys. Rev. B **41**, 8593 (1990).